Pattern Recognition 43 (2010) 2418–2427

Contents lists available at ScienceDirect

Pattern Recognition

journal homepage: www.elsevier.com/locate/pr

A topology preserving non-rigid registration algorithm with integration shape knowledge to segment brain subcortical structures from MRI images

Xiangbo Lin [a,b,*], Tianshuang Qiu [a], Frederic Morain-Nicolier [b], Su Ruan [b]

[a] School of Electronic and Information Engineering, Dalian University of Technology, Dalian 116024, China
[b] Department GE&II, IUT de Troyes, Université de Reims Champagne-Ardenne, 10026 Troyes Cedex, France

ARTICLE INFO

Article history:
Received 11 March 2009
Received in revised form
20 October 2009
Accepted 19 January 2010

Keywords:
Non-rigid registration
Topology preservation
Shape registration
Multi-objects segmentation

ABSTRACT

A new non-rigid registration method combining image intensity and a priori shape knowledge of the objects in the image is proposed. This method, based on optical flow theory, uses a topology correction strategy to prevent topological changes of the deformed objects and the a priori shape knowledge to keep the object shapes during the deformation process. Advantages of the method over classical intensity based non-rigid registration are that it can improve the registration precision with the a priori knowledge and allows to segment objects at the same time, especially efficient in the case of segmenting adjacent objects having similar intensities. The proposed algorithm is applied to segment brain subcortical structures from 15 real brain MRI images and evaluated by comparing with ground truths. The obtained results show the efficiency and robustness of our method.

1. Introduction

In recent years, the analysis of anatomical structures and substructures from medical images develop rapidly [1,2] due to the widespread research on brain functions and brain disorders. Brain internal structures play a central role in the intellectual capabilities of the human brain. Additionally, these structures are also relevant to a set of clinical conditions, such as Parkinson's and Creutzfeldt-Jakob diseases. However, segmenting these structures from MRI images remains a challenging task due to their complex shapes, partial volume effects, anatomical variability, and the lack of clearly defined edges.

A variety of computer-assisted methods have been studied to automatically segment brain internal structures [3–9]. We can cite deformable models or active contour evolution based methods [4,5,7], which can be good solutions to the problem because of their abilities to capture the information of the shapes or structures of interest. Although combining a registration process would be good solutions to the initialization problem [7], such methods still suffer from poor image contrast and missing boundaries. Methods based on expert or atlas knowledge are very attractive to make segmentation automatic [8,10]. In [8], the authors use information fusion to combine medical expertise with fuzzy maps of morphological, topological, and tissue composition data for anatomical structures segmentation in brain MRIs. In [10], a fuzzy model was introduced to represent more appropriately the knowledge of distance, shape and relationship of structures mainly derived from an anatomic atlas. Then a precise labeling of the desired structures is achieved using GAs followed by a voxel-wise amendment using parallel region growing. The published experiment results confirmed the value of knowledge integration in image segmentation and labeling. Another crucial technology is registration based image segmentation methods [1,6,9,11,12], referred to as registration-segmentation. These methods rely on a reference image volume with a corresponding atlas in which structures of interest have been carefully segmented by experts. To segment a new image volume, a transformation that registers the reference volume to the target volume is computed, which gives a spatial correspondence between the two image volumes. Then regions labeled in the atlas can be projected onto the volume of interest using the obtained transformation. Hence the segmentation problem is converted to a registration problem. These methods take advantage of the prior knowledge provided by the atlas (structure shape, relative positions between the structures and so on). Such strategy is helpful to the segmentation of the anatomical structures which are not clearly defined in the input images. The proposed method is based on this type of method.

The key of such registration-segmentation methods is to ensure the obtained spatial transformation accurate, robust and physically reasonable, where the topology preservation is an important constraint. Topology preservation means the unchanged connectivity inside a structure and the relationships between the neighboring structures in the deformed image. There is no tearing, no folding and no appearance or disappearance of structures. By adding this constraint on the deformation field, the optimal solution space can

* Corresponding author at: School of Electronic and Information Engineering, Dalian University of Technology, Dalian 116024, China.
E-mail addresses: linxbo@dlut.edu.cn (X. Lin), qiutsh@dlut.edu.cn (T. Qiu), frederic.nicolier@univ-reims.fr (F. Morain-Nicolier), su.ruan@univ-reims.fr (S. Ruan).

0031-3203/$ - see front matter © 2010 Elsevier Ltd. All rights reserved.
doi:10.1016/j.patcog.2010.01.012

be limited to physically accepted ones. Topology preservation can be generally implemented by ensuring a positive Jacobian of the transformation [13–16]. One way to enforce topology preservation consists in adding further constraints on the deformation model such as penalization of small Jacobian values [9,15–17]. Another way is to track the Jacobian during the registration procedure [18,19]. Here we preserve the topology of a transformation using a local displacements correction method based on analyzing the geometrical features of a vector field.

In this paper, a new non-rigid registration method based on optical flow theory combining both image intensity and structure shape information is proposed to segment the brain MRI internal structures. The main contributions of the proposed method are twofold: (1) a new designed cost function, which combines *a priori* shape knowledge with the intensity information, and is represented efficiently by a distance map; and (2) a topology correction strategy, which ensures the consistency of the vector field obtained by optical flow based registration. This paper is organized as follows. In Section 2 the principle of the intensity based non-rigid registration is described. Based on this principle, the proposed method is presented in detail in Section 3. Then experimental results on MRI images are shown in Section 4. In Section 5, the conclusion is finally given.

2. Intensity based non-rigid registration

Image registration is a well studied problem [20–24]. This problem can be described as finding an optimal spatial transformation $\boldsymbol{T}^*$ for matching the transformed reference image to the target image. In addition to intensities, the positions should be considered for image data in image processing. A transformation $\boldsymbol{T}$ is a spatial mapping that relates the position of features in one image or coordinate space with the position of the corresponding features in another image or coordinate space. In general the optimal transformation $\boldsymbol{T}^*$ is acquired by minimizing the overall cost function E:

$$\boldsymbol{T}^* = \arg\min_{\boldsymbol{T}\in\Gamma}\{E(\boldsymbol{T})\} = \arg\min_{\boldsymbol{T}\in\Gamma}\{E_{sim}(B, A\circ\boldsymbol{T}) + E_{reg}(\boldsymbol{T})\} \tag{1}$$

where A and B denote the reference image and the target image respectively. The set Γ is the space of admissible transformations. $E_{sim}(B, A\circ\boldsymbol{T})$ as the first part of E denotes the data similarity measure and $E_{reg}(\boldsymbol{T})$ as the second part denotes the regularization term to penalize the undesirable transformations.

Different features can be used to construct the similarity measure among which the sum of squared differences (SSD) is a simpler one. The formulation of such metric is

$$E_{sim}(B, A\circ\boldsymbol{T}) = E_{SSD}^{intensity}(B, A\circ\boldsymbol{T}) = \tfrac{1}{2}\|B - A\circ\boldsymbol{T}\|^2 \tag{2}$$

The SSD forms the basis of the intensity-based image registration algorithms and the optimal solution can be obtained by classical optimization algorithms. Among many different intensity based non-rigid image registration algorithms, the Demons algorithm (using SSD metric) [25] and its variants [26–28] are proved to be one of the most efficient methods. As is well known, a simple optimization of Eq. (2) over the space of non-parametric transformations leads to unstable and non-smooth solutions. The added regularization term $E_{reg}(\boldsymbol{T})$ is exactly used to overcome such problem. Here the defined regularization term is

$$E_{reg}(\boldsymbol{T}) = q||\nabla\boldsymbol{T}||^2 \tag{3}$$

where q controls the amount of regularization. Therefore, the cost function can be written as

$$E = E_{sim}(B, A\circ\boldsymbol{T}) + E_{reg}(\boldsymbol{T}) = E_{SSD}^{intensity}(B, A\circ\boldsymbol{T}) + E_{reg}(\boldsymbol{T}) = \tfrac{1}{2}\|B - A\circ\boldsymbol{T}\|^2 + q||\nabla\boldsymbol{T}||^2 \tag{4}$$

However, Eq. (4) will in general lead to computational intensive optimization steps. Ref. [25] provides a very ingenious scheme that optimizes the data similarity measure and the regularization term alternately. In this scheme, the deformation field is regularized by simple Gaussian smoothing. The details of the regularization problems can be found in [20]. On the other hand, the optimization of the data similarity term can be studied from the viewpoint of optical flow theory. Under the assumption of intensity preservation, the image moving velocity $\boldsymbol{v}$ is computed. Generally $\boldsymbol{v}$ is considered simply as a displacement vector field $\boldsymbol{u} = -\boldsymbol{v}$ in image registration problem. Then at each point $\boldsymbol{p}$ of the image, the displacement vector is

$$\boldsymbol{u}(\boldsymbol{p}) = -\frac{(A\circ\boldsymbol{T}(\boldsymbol{p}) - B(\boldsymbol{p}))}{(A\circ\boldsymbol{T}(\boldsymbol{p}) - B(\boldsymbol{p}))^2 + \|\nabla B(\boldsymbol{p})\|^2}\nabla B(\boldsymbol{p}) \tag{5}$$

The detailed derivation of the displacement vector field can be found in [25].

In summary, the optimization process of the spatial transformation is an alternately iterative process. The main steps can be described by the following iterations:

(a) Given the current transformation $\boldsymbol{T}(n)$, compute the displacement field $\boldsymbol{u}(n)$.
(b) Smooth the displacement field $\boldsymbol{u}(n)$: $\boldsymbol{u}(n) \leftarrow G_\sigma * \boldsymbol{u}(n)$, where G_σ is Gaussian smoothing filter.
(c) Compute the new transformation $\boldsymbol{T}(n+1) \leftarrow \boldsymbol{T}(n) + \boldsymbol{u}(n)$.

3. Method

It can be seen from Eq. (4) that only image intensity information is used in the cost function for matching under the constraint of a smooth deformation field. It is enough in some applications when the multi homologous objects in the two images do not have a large deformation. However it is insufficient in some situations. For example, if only a narrow gap exists between two objects with very similar intensities in the target image, and if one of the corresponding objects in the reference image overlaps with both the two target objects, a split problem will occur. Such situation is not a particular case and is common especially for brain deep gray structures. The final registration result might be good in visual inspection for such cases if we only see image intensities. However, if we follow up the displacements of the points on the structures, the corresponding points after the transformation could not correctly represent the structures. Therefore some complementary information must be taken into account. Features extracted by special feature extraction algorithms, such as points, lines and surfaces, are commonly used as the complementary information. The hybrid intensity and feature based techniques integrate the strengths of both intensity and feature based registration method, which would be favorite to many applications [28–30].

3.1. Combined intensity with shape non-rigid registration

An atlas of the structures superposed on the reference image, can provide a priori knowledge, such as the shapes of the structures, the relative positions between them. In common sense, homologous subcortical structures among normal subjects should have similar shapes. Therefore adding a shape similarity term in the cost function would be reasonable. To achieve the goals, an appropriate representation for the shapes of interest is important. Inspired by [10,31,32], we choose the distance transform to represent the shape of interest. The role of a distance function in improving registration quality has been mentioned in

other early work, such as [33], where a chamfer distance function was used for the improvement of sulcal-based registration.

Let $\Phi_S : \Omega \to R^+$ be a distance transform of a shape S, which defines a partition of the image domain Ω. Let ω denote the region that is enclosed by S, and $\Omega-\omega$ denote the background region, the shape representation will be

$$\Phi_S(\boldsymbol{p}) = \begin{cases} 0, & \boldsymbol{p} \in S \\ d(\boldsymbol{p}, S), & \boldsymbol{p} \in \omega \\ -d(\boldsymbol{p}, S), & \boldsymbol{p} \in \Omega-\omega \end{cases} \tag{6}$$

Where $d(\boldsymbol{p}, S)$ refers to the minimum distance between image point $\boldsymbol{p}$ and the shape S. Here Euclidean distance is used as the distance metric. Fig. 1 is an example of the shape representation. Here Fig. 1(a) represents the shape of the putamen in one brain MRI slice and Fig. 1(b) is its corresponding distance representation map using Euclidean distance. Darker the intensity is, farther away the distance from the edge of the putamen. This distance map allows one to get a deformation measure compared to the original shape. It can be easily proved that the gradient vector of the shape distance map is in the normal direction of the shape.

This representation provides supplementary shape information related to the intensity image that can be conveniently used as a new similarity term

$$E_{SSD}^{shape}(\Phi_S(A), \Phi_S(A \circ \boldsymbol{T})) = \tfrac{1}{2}\|\Phi_S(A \circ \boldsymbol{T}) - \Phi_S(A)\|^2 \tag{7}$$

Where $\Phi_S(A)$ is the shape representation of the structure in the atlas on the reference image A and $\Phi_S(A \circ \boldsymbol{T})$ is the shape representation of the corresponding structure in the deformed atlas after the transformation $\boldsymbol{T}$. Under the constraint of the shape similarity term, the optimal transform would lead to the final segmented structure shape as closer as that in the atlas. Therefore the above overall cost function can be modified as

$$E = E_{sim}(B, A \circ \boldsymbol{T}) + E_{reg}(\boldsymbol{T}) = E_{SSD}^{intensity}(B, A \circ \boldsymbol{T}) + E_{SSD}^{shape}(\Phi_S(A), \Phi_S(A \circ \boldsymbol{T})) + E_{reg}(\boldsymbol{T}) \tag{8}$$

By extending the original Demons registration algorithm [25], an optimal solution can be obtained by the alternating strategy. The displacement vectors related to the intensity and the shape at the point $\boldsymbol{p}$ of interest regions are

$$\boldsymbol{u}_{intensity}(\boldsymbol{p}) = -\frac{(A \circ \boldsymbol{T}(\boldsymbol{p}) - B(\boldsymbol{p}))}{(A \circ \boldsymbol{T}(\boldsymbol{p}) - B(\boldsymbol{p}))^2 + \|\nabla B(\boldsymbol{p})\|^2} \nabla B(\boldsymbol{p}) \tag{9}$$

$$\boldsymbol{u}_{shape}(\boldsymbol{p}) = -\frac{(\Phi_S(A \circ \boldsymbol{T}(\boldsymbol{p})) - \Phi_S(A(\boldsymbol{p})))}{(\Phi_S(A \circ \boldsymbol{T}(\boldsymbol{p})) - \Phi_S(A(\boldsymbol{p})))^2 + \|\nabla \Phi_S(A(\boldsymbol{p}))\|^2} \nabla \Phi_S(A(\boldsymbol{p})) \tag{10}$$

The combined displacement vector is

$$\boldsymbol{u}(\boldsymbol{p}) = (1-\beta)\boldsymbol{u}_{intensity}(\boldsymbol{p}) + \beta \boldsymbol{u}_{shape}(\boldsymbol{p}) \tag{11}$$

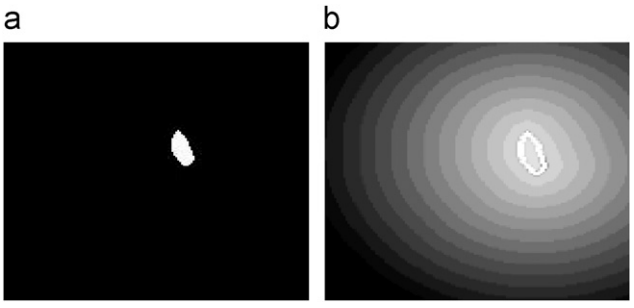

Fig. 1. An example of the shape representation (a) the putamen (b) its shape distance representation map.

Here the parameter $\beta \in [0, 1]$ is used to balance the contribution of the intensity metric and the shape metric: $\beta = 0$ means a pure intensity contribution and $\beta = 1$ means a pure shape contribution.

A simple piecewise linear function is used to adjust adaptively the weight of the parameter, which is depicted in Fig. 2. The symbols used in Fig. 2 are as follows:

x: the intensity I of the target image in the region of interest.
$x_0 = mean(I_{structure})$: the average intensity of the structure region enclosed by the boundary of the deformed atlas structure.
$x_0^- = x_0 - \lambda\sigma_{structure}$ and $x_0^+ = x_0 + \lambda\sigma_{structure}$: key intensity values where the intensity metric and the shape metric have the same importance. Herein $\sigma_{structure}$ denotes the intensity standard deviation of the structure region enclosed by the boundary of the deformed atlas structure. λ is an empirical parameter to control the dynamic intensity range in which the shape metric is more or less important than the intensity metric according to the intensity value near to or far from the intensity mean x_0.

In our previous preliminary work [34], the structure of interest was registered and segmented one by one sequentially. Such procedure was time consuming, especially for multi-structures segmentation. Here an improvement is proposed. The new strategy can register and segment multi-objects with very similar intensities in one time. Let s_i, $i = 1, \ldots, N$ be N different structures of interest. At any point $\boldsymbol{p}$, the shape representation of s_i is $\Phi_{S_i}(\boldsymbol{p})$. Then the N different shape representations are integrated into a unified shape map $M(\boldsymbol{p})$ according to the following principles:

$$M(\boldsymbol{p}) = \begin{cases} \Phi_{s_i}(\boldsymbol{p}) & \text{if } \Phi_{s_i}(\boldsymbol{p}) \geq 0 \\ \max(\Phi_{s_i}(\boldsymbol{p})) & \text{if } \Phi_{s_i}(p) < 0 \text{ and } |\max(\Phi_{s_i}(\boldsymbol{p}))| \leq \varepsilon \\ 0 & \text{if } \Phi_{s_i}(p) < 0 \text{ and } |\max(\Phi_{s_i}(\boldsymbol{p}))| > \varepsilon \end{cases} \tag{12}$$

where ε is the threshold, $\varepsilon = \min_i\{\max_p(\Phi_{s_i}(\boldsymbol{p}))\}$. Therefore, $\Phi_S(\bullet)$ in Eqs. (7), (8) and (10) should be replaced by $M(\bullet)$ in the implementation procedure.

3.2. Topology correction strategy

As is mentioned, topology preservation of a deformation field is important in registration-segmentation method for normal brain case. Although bijectivity and smoothing techniques adopted in optimizing the cost function like Eq. (4) or (8) can be helpful for preventing topology change, it is hard to be verified in theory. The topology preservation problem of the Demons algorithm has been investigated in recent years [35–37]. Some cases without topology preservation using this method have been found in some published reliable experiments [35] and our experiments. By optimizing the cost function over a space of diffeomorphism, a diffeomorphic Demons algorithm was proposed [36,37]. In this paper, a different simple topology correction method is proposed based on the vector field analysis.

Let $\boldsymbol{T} = (X, Y, Z)$ denote the deformation field, where (X, Y, Z) is the new position of point $\boldsymbol{p}$ (x, y, z) after deformation. Then its

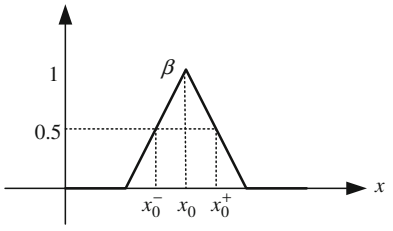

Fig. 2. The function of the balance parameter β.

Jacobian at point $\boldsymbol{p}$ is

$$J_T(\boldsymbol{p}) = \det[\partial X/\partial x \;\; \partial X/\partial y \;\; \partial X/\partial z;\;\; \partial Y/\partial x \;\; \partial Y/\partial y \;\; \partial Y/\partial z;\;\; \partial Z/\partial x \;\; \partial Z/\partial y \;\; \partial Z/\partial z] \tag{13}$$

A topology preservation deformation field must satisfy $J_T(\boldsymbol{p}) > 0$ at any point.

3.2.1. Deformation field analysis

The obtained deformation field in image registration is a vector field from Eq. (4), which reflects the spatial transformation between the corresponding structures in the two images. To improve the understanding of the underlying physical procedure and the implied topology information described by the deformation field, it is useful to analyze the characteristics of the vector field. A vector field can be characterized by its critical points [38]. The most important critical points are attractors, repellors and vortices, which are depicted in Fig. 3.

The displacement vector field is a function of the gradient of a scalar field according to Eq. (5). In this discussed deformation field, only attractors and repellors are considered because of the irrotationality of a gradient vector field. The critical points of the vector field represent different physical properties, which is dependent on the applications. For inter-subject brain MRI image registration, the attractors characterize the expansion of the corresponding brain structures, while the repellors characterize the contraction. Such intrinsic relationship coincides with the relationship between the Jacobian and the real physical properties. $J_T > 1$ means the expansions of the brain structures, $J_T < 1$ means the contractions, $J_T = 1$ means volume preservations and $J_T \leq 0$ means the changed topologies [16,38,39]. As is mentioned above, topology violation induced by image deformation mainly shows tears or overlaps. According to the diagrammatic characteristics of the critical points (Fig. 3), it is easy to see that overlaps due to extrusions or folds will occur in attractors and tears due to over expansions will occur in repellors. The common situations in 2D are shown in Fig. 4.

The numbers 1, 2, 3, 4 in Fig. 4 represent the four vertexes of an initial rectangle grid. The thick line denotes the deformed grid, whose vertexes numbered 1′, 2′, 3′, 4′. They correspond to the initial four points. The dashed line represents the deformation path of each vertex. It can be seen from Fig. 4(a) that overlap due to folds occurs during the deformation procedure, just like a plane not only changed in the shape but also reversed. Fig. 4(b) depicts the overlap due to extrusions, where points 2 and 3 cross in the

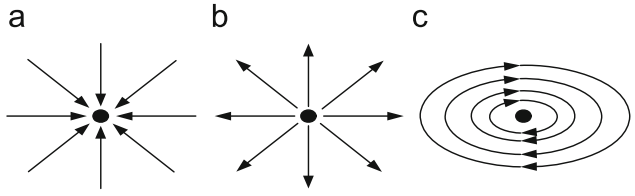

Fig. 3. Important critical points of a vector field: (a) attractor; (b) repellor and (c) vortice.

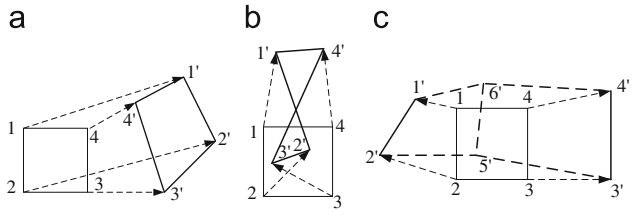

Fig. 4. Paradigm of the changed topology in 2D space due to the deformations: (a) fold; (b) overlap and (c) tear.

deformation procedure and the grid twists. Fig. 4(c) depicts the tears because of the over expansions that exceed the permitted tension strength. Here 5′ and 6′ are new inserted points coming from surrounding regions to fill the gap.

It can be clearly seen that if the displacement magnitudes of the adjacent points along the primary deformation direction are not suitable, the new position of the point behind overlaps the new position of the point ahead after deformation, folds will occur. If the deformation directions of the adjacent points near the attractors are opposite and they have unexpected large displacement magnitudes, crosses will occur. Therefore both intuitive and easy solutions are to change such points' displacements in a proper way in order to preserve the topologies, where the prerequisite is to preserve the geometrical features of the original deformation fields as much as possible.

3.2.2. Correction strategies

If a continuously differentiable deformation field is topology preservation, its Jacobian should be positive everywhere in its domain. A digital image limited by the resolution is defined in the discrete grid, which is not a continuous function. So the corresponding deformation field is discrete. As is mentioned in Ref. [40], if a continuous deformation field is determined by its discrete counterpart via the bilinear interpolation, its characteristics depend on the discrete deformation field. Therefore, if the Jacobians of various discrete grid points of the discrete deformation field are positive, its continuous counterpart preserves topology in its domain.

Let a continuous deformation field be described as

$$X(x,y,z) = x + u^x(x,y,z) \tag{14}$$

$$Y(x,y,z) = y + u^y(x,y,z) \tag{15}$$

$$Z(x,y,z) = z + u^z(x,y,z) \tag{16}$$

where $u^x(x,y,z)$, $u^y(x,y,z)$ and $u^z(x,y,z)$ are the displacement field components of a point $\boldsymbol{p}(x,y,z)$ along xyz axes. The Jacobian of the point $\boldsymbol{p}(x,y,z)$ is $J(x,y,z)$. Define another deformation field $\boldsymbol{T}_k$ as

$$X_k(x,y,z) = x + ku^x(x,y,z) \tag{17}$$

$$Y_k(x,y,z) = y + ku^y(x,y,z) \tag{18}$$

$$Z_k(x,y,z) = z + ku^z(x,y,z) \tag{19}$$

Let $J_k(x,y,z)$ denote the Jacobian of $\boldsymbol{T}_k$ at point $\boldsymbol{p}(x,y,z)$. It is easy to see that when $k=0$, $J_k(x,y,z)=1$ and when $k=1$, $J_k(x,y,z)=J(x,y,z)$. If the Jacobian of $\boldsymbol{T}_k$ at point $\boldsymbol{p}(x,y,z)$ is $J(x,y,z)<0$, the topology preservation is violated. From the continuity of $J_k(x,y,z)$ with respect to k, there exists $k^* \in [0,1]$ such that $J_{k^*}(x,y,z) > 0$. Because sampling a continuous deformation field results in a discrete deformation field, the topology attributes of a discrete deformation field can be corrected by multiplying a proper factor between 0 and 1 in the original displacement field. According to Eq. (13), the Jacobian of a deformation field is related to its gradient. Here central-difference method [41] is adopted to compute the discrete gradients. Those points situated in both sides of the central point are named association points.

3.3. Algorithm

In summary, given a reference image A with its pre-labeled image (the atlas) and the target image B, the overall registration procedure is proposed as follows (after the brain extraction):

1. Initializing A by a global registration by FSL [42].

2. Performing the intensity based Demons non-rigid registration between the global transformed reference image A and the target image B with the following topology correction for the obtained deformation field:
   (1) Computing $J(x,y,z)$ of each point according to the obtained deformation field;
   (2) Decreasing the k value from $k=1$ with a same step if $J(x,y,z)<0$, and the new displacements of the association points around the central point (x,y,z) will be acquired. Computing $J_k(x,y,z)$ according to the new displacements. Repeating it until the proper k^* is found, such that for all points of the deformation field, $J_{k^*}(x,y,z)>0$;
   (3) Evaluating the similarity between the deformed reference image by the obtained $\boldsymbol{T}_{k^*}$ and the target image. If the result does not meet the requirement, change the reference image with the obtained deformed reference and register again.
3. Performing the proposed non-rigid registration algorithm with integration shape knowledge to refine the match of subtle structures. This refinement allows resolving the narrow gap problem existing between two objects with very similar intensities. Similarly a topology correction as described in step 2 is applied to the obtained deformation field.

4. Experiments and results

The proposed non-rigid registration algorithm aims to segment multi-objects having very similar intensities in images simultaneously. In this paper only T1 weighted brain MRI images is used because of its good intensity contrast of the structures. Topology preservation of the proposed algorithm makes many benefits for this aim. It maintains the integrality of a deformed object and prevents the appearance or disappearance of objects as much as possible. Another contribution of the proposed algorithm is that a shape similarity metric based on distance map is integrated to the classical intensity based non-rigid registration algorithm. It makes the segmentation of adjacent objects having similar intensities more accurate and automatic.

The proposed algorithm is tested by segmenting the brain subcortical structures from MRI images. The reference image used in the experiment is the one offered from the Surgical Planning Laboratory of Harvard Medical School [43]. It consists of $256\times256\times160$ voxels with a spatial resolution of $0.9375\,\text{mm}\times0.9375\,\text{mm}\times1.5\,\text{mm}$. The test images are real brain MRI images of 15 normal subjects provided by the Center for Morphometric Analysis at Massachusetts General Hospital and available from Internet Brain Segmentation Repository (IBSR) [44].

As is mentioned in [25], if the two objects to be matched do not overlap, the Demons algorithm is inefficient. So a fast global registration and an image intensity match procedures should be performed before the Demons non-rigid registration. Here we firstly use the software FSL [42] to do the initial registration.

In the experiment, one should remember that the combined intensity and shape non-rigid registration is performed only on structures of interest. The additional transform of structures should influence other regions as little as possible. Therefore a region of interest selection must be done before refinement according to Eq. (12). The selection of the parameter λ is to be mentioned. It can be seen from Fig. 2 that the parameter β varies with intensities of structures. Therefore only parameter λ is constant and will be determined empirically. Its value is not arbitrary but is easy to find a convenient one. Because a relative good intensity match has been obtained after the previous registration, more weightiness should be given to the shape metric. Hence a larger parameter λ should be convenient. We set it to be 0.7 in our experiments for all cases.

The experiment results in Fig. 5 show some cases of topologic changes after using a classical Demons registration which uses only bijectivity and smooth techniques. The Jacobians are not

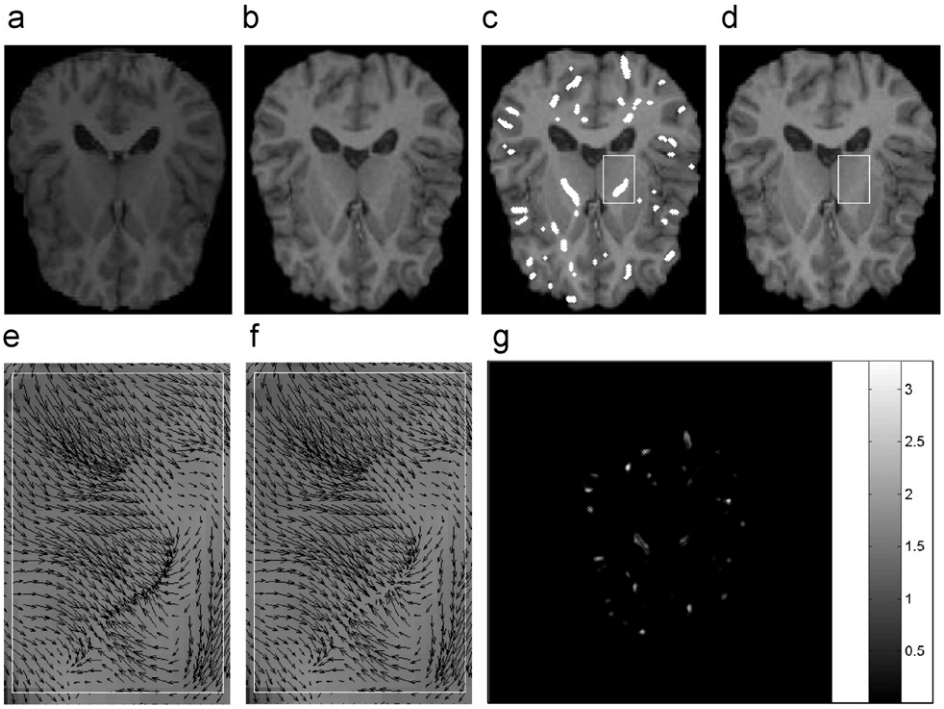

Fig. 5. Comparisons of the deformation fields between registration with and without topology correction strategy: (a) the template image; (b) the target image; (c) the deformed template image based on the deformation field without topology correction; (d) the deformed template image based on the deformation field with topology correction; (e) the enlarged highlight region of (c); (f) the enlarged highlight region of (d) and (g) the magnitude differences of the two deformation fields with and without topology correction.

positive in some regions in these cases. The deformable reference image and the target image are showed in Fig. 5(a) and (b), respectively, while Fig. 5(c) is the deformed reference image by the deformation field without topology correction. It can be seen that the similarity between the deformed reference image and the target image is high in visual inspection. The white parts in

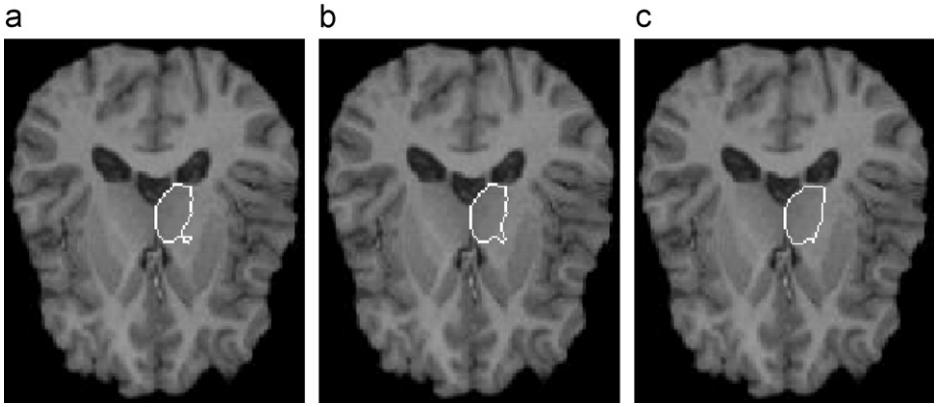

Fig. 6. Exemplifications of the proposed contributions (a) no topology correction and shape knowledge are used; (b) only topology correction is used and (c) both topology correction and shape knowledge are used.

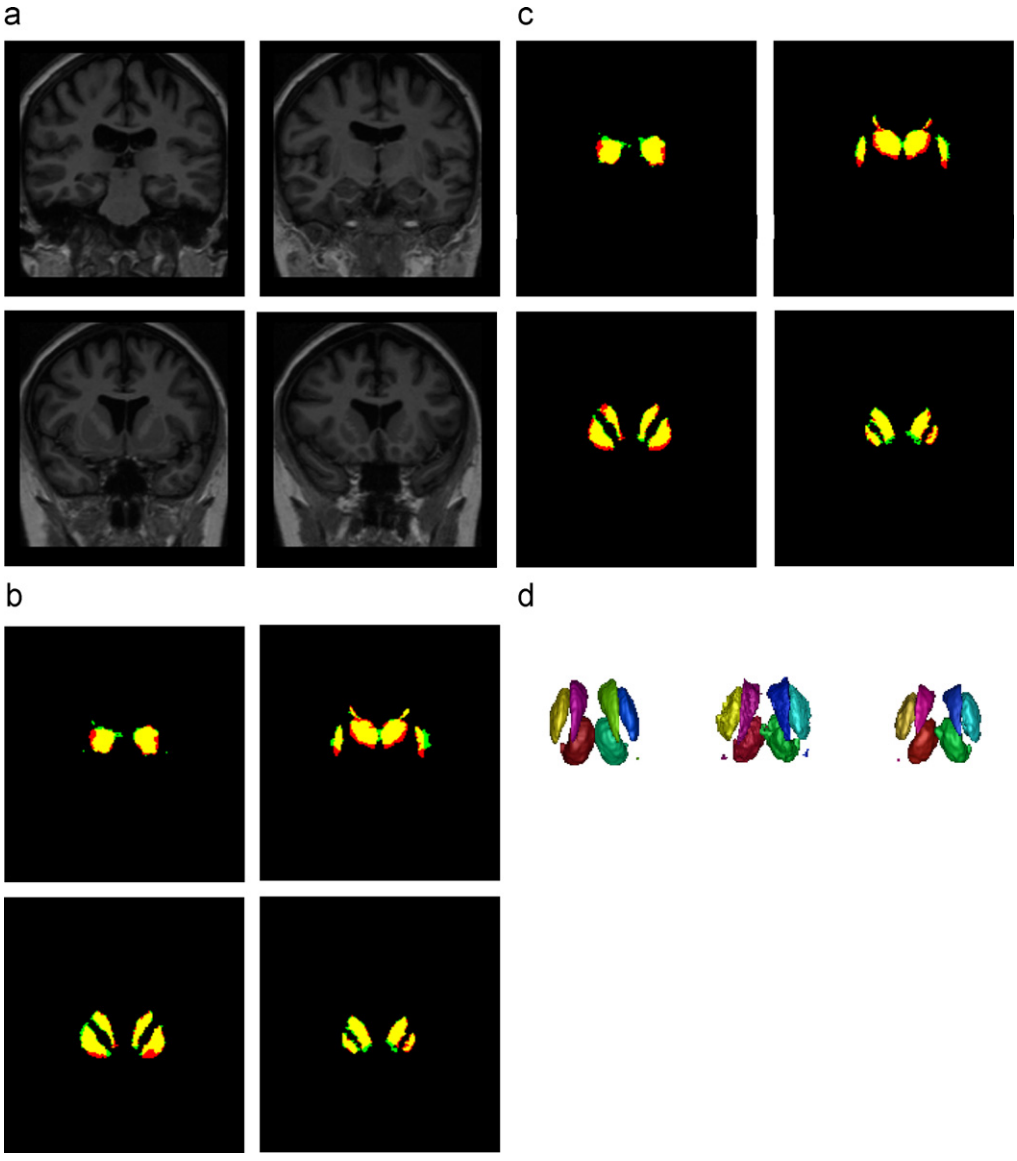

Fig. 7. Segmentation results comparison between the original Demons algorithm and the proposed method: (a) MRI image; (b) segmentation using the original method; (c) segmentation using the proposed method and (d) 3D views (left—ground truth, middle—original method, right—the proposed method).

Fig. 5(c) represent the positions with negative Jacobians in the deformation field, which means the topology violation in these positions. One typical region with changed topologies is highlighted using white rectangle. The enlarged deformation field diagram of the highlighted region is depicted in Fig. 5(e), where crosses can be observed near the attractors. Fig. 5(d) is the deformed reference image by the deformation field with topology correction, where the same region as in Fig. 5(c) is highlighted and its enlarged diagram is depicted in Fig. 5(f). The disappeared white parts in Fig. 5(d) indicate that the Jacobians of the topology corrected deformation field satisfy the topology preservation requirements. Compared to Fig. 5(e), the deformation field with topology preservation (Fig. 5(f)) is more regular and much smoother. In the experiments, the parameter k changes with a step of 0.01. If the cross correlation between the deformed reference image and the target image equals or exceeds the set threshold or the passes of re-registration using the deformed image as the new reference image reach the upper limit (here it is three), the algorithm will stop. Here the cross correlation threshold is $CC_t=(1-CC_0)/\alpha+CC_0$, where CC_0 is the initial cross correlation between the reference and the target images. The value of 1.2 is suitable for parameter α in the experiment. Fig. 5(g) is the magnitude differences of the two deformation fields with and without topology correction. The brighter the intensity is, the larger the difference is. Here the averaged max difference is 2.18 pixels, which means the corrected deformation field is generally able to preserve the original properties of the deformation field.

Fig. 6 describes the influences of the topology preservation and the a prior shape knowledge to the object segmentation. The segmentation results of the thalamus based on different strategies are depicted in Fig. 6(a)–(c), respectively, where (a) shows the result in the case of no topology correction and shape knowledge being used, (b) shows the result in the case of only topology correction being used and (c) shows the result in the case of both topology correction and shape knowledge being used. Obviously, the segmentation in Fig. 6(c) is better than the other two. It can be seen that tears occur in Fig. 6(a). Though correcting the topology of the deformation field can preserve the object's topology, it

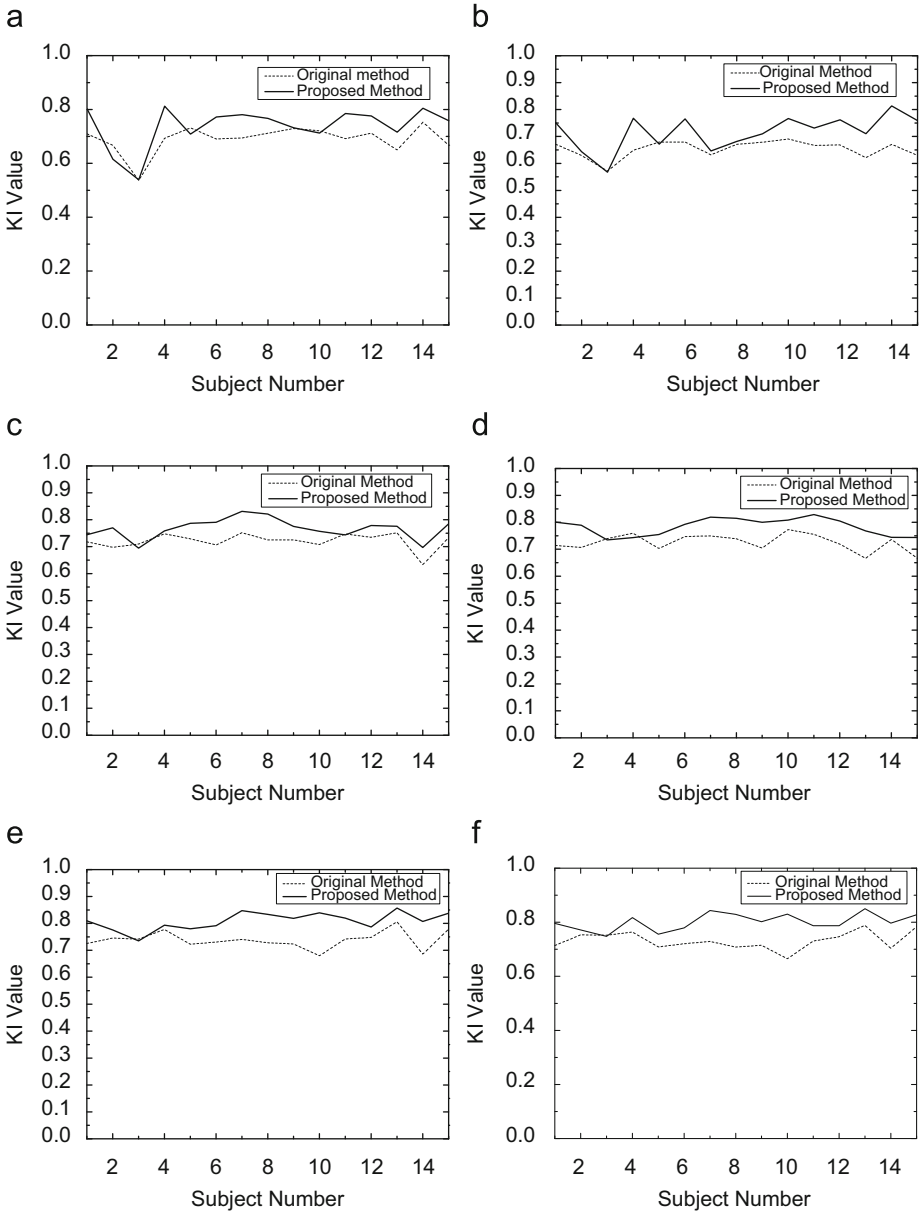

Fig. 8. Comparisons of KI values: (a) left caudate; (b) right caudate; (c) left putamen; (d) right putamen; (e) left thalamus and (f) right thalamus.

cannot ensure a satisfied segmentation, which is shown in Fig. 6(b). Under the joint constrains of the intensity and the shape knowledge, as well as the topology correction procedure, a better segmentation is obtained in Fig. 6(c).

Comparative studies between the original Demons method and the proposed method are carried out by segmenting brain internal structures from all volumes. Fig. 7 shows some typical slices of one volume, which provides an intuitive way to evaluate the segmentation. Fig. 7(a) is the target image and the segmentation results using the original Demons algorithm and the proposed method are depicted in Fig. 7(b) and (c), respectively. The figure shows three colors. The red color describes the 'ground truth' segmentations, which are provided by IBSR database. The green color represents the automatically segmented results and the overlap parts with the 'ground truth' are described in yellow color. The final 3D views are presented in Fig. 7(d). The results show significant improvements, especially in left putamen (top right slice and down left slice), when the proposed method is adopted.

To validate the results quantitatively, the criterion widely used in atlas-based segmentation [2,7,9,45,46], a kappa statistic based similarity index is adopted in this paper. The similarity index measures the overlap ratio between the segmented structure and the ground truth, which is defined as

$$\mathrm{KI} = \frac{2 \times \mathrm{TP}}{2 \times \mathrm{TP} + \mathrm{FN} + \mathrm{FP}} \tag{20}$$

The definitions of the parameters are as follows:

$\mathrm{TP} = G \cap E$: the number of true positive;
$\mathrm{FP} = \overline{G} \cap E$: the number of false positive; and
$\mathrm{FN} = G \cap \overline{E}$: the number of false negative;

where G is the ground truth segmentation of a given structure, E is the estimated segmentation of the same structure, and $\overline{O}$ denotes the complement of a set O. Perfect spatial correspondence between the two segmentations will result in KI=1, whereas no correspondence will result in KI=0.

The KI values are computed for all the structures of all the volumes. The results are presented in Fig. 8, and the associated critical values are summarized in Table 1. The segmented structures are left and right caudate (*L-Caudate, R-Caudate*), putamen (*L-Putamen, R-Putamen*) and thalamus (*L-Thalamus, R-Thalamus*). The proposed method and the original method are represented by 'Pro.' and 'Ori.' in Table 1, respectively. The 'max', 'min', 'mean' and 'SD' items list the maximum, minimum, mean and standard deviation of KI values counted from all volumes. These results indicate that in most cases, the proposed method gives better segmentations than the original method. As is known, the brain subcortical structures have relatively small sizes, complex shapes. Moreover, there is only small spacing between different structures, while their intensities in MRI images are very similar. All these negative factors make the fully automatically accurate segmentation a challenging task. As explained in [47], a value of KI >0.7 indicates a strong agreement. So the results are satisfactory as the KI of the segmented structures is larger than 0.7 for almost all 15 cases.

We also compared our structures segmentation results with those using original Demons algorithm and those reported in [9,17], because all the adopted algorithms belong to registration-segmentation method and the used validation data are from the same public database. In [9], the validation criterion is the same as Eq. (20) and the results were averaged on 34 structures. While the validation criterion in [17] named the relative overlap (RO) is different, which is defined as

$$\mathrm{RO} = \frac{G \cap E}{G \cup E} \times 100 \tag{21}$$

The comparison results are presented in Tables 2 and 3, respectively. It can be seen that both the validation criteria indicate a better segmentation of the proposed algorithm than that of the Demons registration. And the obtained KI value reaches the best result in [9] well, while the standard deviation (SD) is much smaller, which means a more robust segmentation for different data. Table 3 depicts the comparison of the RO value between our results and the results published in [17], where 'best' and 'worst' mean the best results and the worst results of the involved algorithms in [17]. As it can be seen, our results are inferior to those published in [17]. Nevertheless, there are too many parameters to be selected in [17], which is a challenge for unskilled users.

Table 1
The KI value for the target segmentation.

Structure	*L-caudate*		*R-caudate*		*L-putamen*		*R-putamen*		*L-thalamus*		*R-thalamus*	
Method	Pro.	Ori.	Pro.	Ori.	Pro.	Ori.	Pro.	Ori.	Pro.	Ori.	Pro.	Ori.
Max	0.812	0.729	0.813	0.691	0.831	0.752	0.829	0.759	0.857	0.806	0.850	0.788
Min	0.539	0.537	0.567	0.571	0.694	0.633	0.743	0.666	0.735	0.680	0.747	0.665
Mean	0.739	0.699	0.717	0.658	0.767	0.725	0.783	0.739	0.809	0.740	0.801	0.730
SD	0.072	0.049	0.062	0.031	0.037	0.029	0.031	0.027	0.031	0.032	0.030	0.032

Table 2
Comparison of averaged KI value between our results and the results published in [9].

Method	Ref. [9]							Ours	
	B_{topo}	B	$B_{0.5<J<2}$	$B_{\mathrm{topo}(\lambda=1)}$	D_{Itk}	$D_{10-\mathrm{JHGM}}$	Affine	Proposed	D_{mat}
KI (SD)	0.765 (0.107)	0.727 (0.152)	0.710 (0.142)	0.777 (0.116)	0.754 (0.105)	0.778 (0.105)	0.627 (0.150)	0.770 (0.064)	0.717 (0.072)

Symbols: B_{topo}—B-spline-based registration with topology preservation and without regularization; B—B-spline-based registration without topology preservation and without regularization; $B_{0.5<J<2}$—B-spline-based registration with the constraint $J_{\min}=0.5$ and $J_{\max}=2$ on the Jacobian and without regularization; $B_{\mathrm{topo}(\lambda=1)}$—B-spline-based registration with topology preservation and with regularization; D_{Itk}—the Demons algorithm based on ITK; $D_{10\text{-JHGM}}$—the Demons algorithm using the intensity normalization; Affine—affine registration with 12 parameters; Proposed—The proposed method in this paper; D_{mat}—the demons algorithm based on our Matlab code.

Table 3
Comparison of RO value between our results and the results published in [17].

Method			*L-caudate*	*R-caudate*	*L-putamen*	*R-putamen*	*L-thalam*	*R-thalam*
Ours	Proposed		58.6	56.3	62.3	65.3	68.2	68.1
	D_{mat}		53.8	49.0	56.9	58.7	58.7	57.5
Ref. [17]	B_{topo}	Best	62.7	–	68.9	–	73.7	–
		Worst	56.7	–	66.4	–	71.5	–
	D_{ltk}	Best	61.3	–	61.0	–	69.4	–
		Worst	54.2	–	56.8	–	67.2	–

Symbols: Proposed—The proposed method in this paper; D_{mat}—the Demons algorithm based on our Matlab code; B_{topo}—B-spline-based registration with topology preservation; D_{ltk}—the Demons algorithm based on ITK.

5. Conclusions

In this paper, a new non-rigid registration algorithm combined intensity and shape knowledge is proposed. It is derived by integrating shape information into a classical intensity based non-rigid registration algorithm. The new added shape metric in the overall cost function provides a remedy to the commonly used SSD intensity metric. Furthermore it has a simple form, is easy to understand and fully automatic. From the perspective of geometrical features of a vector field, the reason causing topological changes is analyzed theoretically. Then a corresponding topology correction strategy to the deformation field is designed, which is important for registration-segmentation problem. The experiment results indicate that the proposed method could be a solution for segmenting multi-objects having very close spacing and similar intensities that lack clearly defined intensity boundaries.

The program is written in Matlab and run on a PC-Windows, Intel core 2 at 1.86 GHz. Without any code optimization, the average processing time for one volume of $256 \times 256 \times 128$ is about 160 min. Therefore one future work should be the run time reduction. Fortunately with the advent of large scale distributed computational infrastructure, the trend of increasing core counts in the face of declining hardware costs, and the optimized code rewritten in a lower-level language such as C, significantly reducing the run time is hopeful. Another future work will be conducting more thorough evaluation by acquiring additional test data from other scanner platforms or pulse sequences, and other imaging modalities.

Acknowledgments

This work is partly supported by National Science Foundation of China (nos. 30570475, 60372081, 60872122).

References

[1] B. Fischl, D.H. Salat, E. Busa, et al., Whole brain segmentation: automated labeling of neuroanatomical structures in the human brain, Neuron 33 (1) (2002) 341–355.
[2] Y. Xia, K. Bettinger, L. Shen, et al., Automatic segmentation of the caudate nucleus from human brain MR images, IEEE Transactions on Medical Imaging 26 (4) (2007) 509–517.
[3] L. Clarke, R. Velthuizen, M. Camacho, et al., MRI segmentation: methods and applications, Magnetic Resonance Imaging 13 (1995) 343–368.
[4] P. Yushkevich, J. Piven, H. Hazlett, R. Smith, et al., User-guided 3-D active contour segmentation of anatomical structures: Significantly improved efficiency and reliability, NeuroImage 31 (2006) 1116–1128.
[5] A. Pitiot, H. Delingette, P. Thompson, N. Ayache, Expert knowledge-guided segmentation system for brain MRI, NeuroImage 23 (2004) 85–96.
[6] D.V. Iosifescu, M.E. Shenton, S.K. Warfield, et al., An automated registration algorithm for measuring MRI subcortical brain structures, NeuroImage 6 (1997) 13–25.
[7] C. Baillard, P. Hellier, C. Barillot, Segmentation of brain 3D MR images using level sets and dense registration, Medical Image Analysis 5 (2001) 185–194.
[8] V. Barra, J.Y. Boire, Automatic segmentation of subcortical brain structures in MR images using information fusion, IEEE Transactions on Medical Imaging 20 (7) (2001) 549–558.
[9] V. Noblet, C. Heinrich, F. Heitz, et al., Retrospective evaluation of a topology preserving non-rigid registration method, Medical Image Analysis 10 (2006) 366–384.
[10] J.-H. Xue, S. Ruan, B. Moretti, et al., Knowledge-based segmentation and labeling of brain structures from MRI images, Pattern Recognition Letters 22 (3–4) (2001) 395–405.
[11] M. George Linguraru, M. Ángel, G. Ballester, N. Ayache, Deformable atlases for the segmentation of internal brain nuclei in magnetic resonance imaging, International Journal of Computers, Communications & Control II (1) (2007) 26–36.
[12] M.G. Linguraru, T. Vercauteren, M. Reyes-Aguirre, et al., Segmentation propagation from deformable atlases for brain mapping and analysis, Brain Research Journal 1 (4) (2007) 1–18.
[13] M. Holden, A review of geometric transformations for nonrigid body registration, IEEE Transactions on Medical Imaging 27 (1) (2008) 111–128.
[14] O. Musse, F. Heitz, J.-P. Armspach, Topology preserving deformable image matching using constrained hierarchical parametric models, IEEE Transactions on Image Processing 10 (7) (2001) 1080–1093.
[15] V. Noblet, C. Heinrich, F. Heitz, J.-P. Armspach, 3-D deformable image registration: a topology preservation scheme based on hierarchical deformation models and interval analysis optimization, IEEE Transactions on Image Processing 14 (5) (2005) 553–566.
[16] A.D. Leow, I. Yanovsky, M.-C. Chiang, et al., Statistical properties of Jacobian maps and the realization of unbiased large-deformation nonlinear image registration, IEEE Transactions on Medical Imaging 26 (06) (2007) 822–832.
[17] M. Sdika, A fast nonrigid image registration with constraints on the Jacobian using large scale constrained optimization, IEEE Transactions on Medical Imaging 27 (2) (2008) 271–281.
[18] A. Trouve′, Diffeomorphisms groups and pattern matching in image analysis, International Journal of Computer Vision 28 (3) (1998) 213–221.
[19] S. Joshi, M. Miller, Landmark matching via large deformation diffeomorphisms, IEEE Transactions on Image Processing 9 (8) (2000) 1357–1370.
[20] J. Modersitzki, Numerical Methods for Image Registration, Oxford University Press, New York, 2004.
[21] P. Zhilkin, M.E. Alexander, J. Sun, Nonlinear registration using variational principle for mutual information, Pattern Recognition 41 (2008) 2493–2502.
[22] D. Shen, Fast image registration by hierarchical soft correspondence detection, Pattern Recognition 42 (2009) 954–961.
[23] E. Haber, S. Heldmann, J. Modersitzki, A computational framework for image-based constrained registration, Linear Algebra and its Applications 431 (2009) 459–470.
[24] E.R. Arce-Santana, A. Alba, Image registration using Markov random coefficient and geometric transformation fields, Pattern Recognition 42 (2009) 1660–1671.
[25] J.P. Thirion, Image matching as a diffusion process: an analogy with Maxwell's demons, Medical Image Analysis 2 (3) (1998) 243–260.
[26] H. Wang, L. Dong, et al., Validation of an accelerated 'demons' algorithm for deformable image registration in radiation therapy, Physics in Medicine and Biology 50 (12) (2005) 2887–2905.
[27] P. Rogelj, S. Kovačič, Symmetric image registration, Medical Image Analysis 10 (3) (2006) 484–493.
[28] P. Cachier, E. Bardinet, et al., Iconic feature based nonrigid registration: the PASHA algorithm, Computer Vision and Image Understanding 89 (2003) 272–298.
[29] P. Cachier, J.-F. Mangin, X. Pennecl, et al., Multisubject non-rigid registration of brain MRI using intensity and geometric features, MICCAI 2001, LNCS 2208 (2001) 734–742.
[30] E. Hellier, C. Barillot, Coupling dense and landmark-based approaches for non-rigid registration, IEEE Transactions on Medical Imaging 22 (2) (2003) 217–227.
[31] X. Huang, N. Paragios, D.N. Metaxas, Shape registration in implicit spaces using information theory and free form deformations, IEEE Transactions on Pattern Analysis and Machine Intelligence 28 (8) (2006) 1303–1318.
[32] A. Tsai, A. Yezzi Jr., W. Wells, et al., A shape-based approach to segmentation of medical imagery using level sets, IEEE Transactions on Medical Imaging 22 (2) (2003) 137–154.

[33] D. Louis Collins, G. Le Goualher, A.C. Evans, Non-linear cerebral registration with sulcal constraints, MICCAI 2 (1998) 974–984.
[34] X.B. Lin, S. Ruan, F. Morain-Nicolier, T.S. Qiu, Non-rigid registration based segmentation of brain subcortical structures using a priori knowledge, in: The Proceedings of the 30th Annual International IEEE EMBS Conference, 2008, pp. 3971–3974.
[35] P. Hellier, C. Barillot, I. Corouge, et al., Retrospective evaluation of intersubject brain registration, IEEE Transactions on Medical Imaging 22 (9) (2003) 1120–1130.
[36] T. Vercauteren, X. Pennec, A. Perchant, N. Ayache, Diffeomorphic demons: efficient non-parametric image registration, NeuroImage 45 (2009) S61–S72.
[37] T. Vercauteren, X. Pennec, A. Perchant, N. Ayache, Non-parametric diffeomorphic image registration with the Demons algorithm,, Medical Image Computing and Computer-Assisted Intervention—MICCAI 2007 4792 (2007) 319–326.
[38] M. Tittgemeyer, G.W. Frithjof Kruggel, Visualising deformation fields computed by non-linear image registration, Computing and Visualization in Science 5 (2002) 45–51.
[39] T. Rohlfing, C.R. Maurer Jr., D.A. Bluemke, M.A. Jacobs, Volume-preserving nonrigid registration of MR breast images using free-form deformation with an incompressibility constraint, IEEE Transactions on Medical Imaging 22 (6) (2003) 730–741.
[40] B. Karaçalı, C. Davatzikos, Estimating topology preserving and smooth displacement fields, IEEE Transactions on Medical Imaging 23 (7) (2004) 868–880.
[41] G.D. Smith, Numerical Solution of Partial Differential Equations: Finite Difference Methods, Oxford University Press, Oxford, 1985.
[42] S.M. Smith, M. Jenkinson, M.W. Woolrich, et al., Advances in functional and structural MR image analysis and implementation as FSL, NeuroImage 23 (S1) (2004) 208–219.
[43] R. Kikinis, et al., A digital brain atlas for surgical planning, model driven segmentation and teaching, IEEE Transactions on Visualization and Computer Graphics 2 (3) (1996) 232–241.
[44] Internet brain segmentation repository, M.G.H. Technical Report, Center for Morphometric Analysis IBSR, 2000 (Online). 〈http://neurowww.mgh.harvard.edu/cma/ibsr〉.
[45] A. Klein, J. Andersson, B.A. Ardekani, Evaluation of 14 nonlinear deformation algorithms applied to human brain MRI registration, NeuroImage 46 (2009) 786–802.
[46] C. Ciofolo, C. Barillot, Atlas-based segmentation of 3D cerebral structures with competitive level sets and fuzzy control, Medical Image Analysis 13 (2009) 456–470.
[47] A. Zijdenbos, B. Dawant, R. Margolin, A. Palmer, Morphometric analysis of white matter lesions in MR images: method and validation, IEEE Transactions on Medical Imaging 13 (4) (1994) 716–724.

About the Author—XIANGBO LIN received the M.S. degree on signal and information processing in Dalian University of Technology, Dalian, China, in 2004. She is currently a Ph.D. student both in the Department of Electronic Engineering, Dalian University of Technology, Dalian, China, and the CReSTIC Laboratory at the University of Reims, France. Her research interests include biomedical engineering, image processing and signal & information processing.

About the Author—TIANSHUANG QIU, received the B.S. degree from Tianjin University, Tianjin, China, in 1983, the M.S. degree from Dalian University of Technology, Dalian, China, in 1993, and the Ph.D. degree from Southeastern University, Nanjing, China, in 1996, all in electrical engineering. He was a research scientist at Dalian Institute of Chemical Physics, Chinese Academy of Sciences, Dalian, China, during 1983 and 1996. He served on the faculty of electrical engineering at Dalian Railway Institute in 1996. He conducted his post-doctoral research in the Department of Electrical Engineering at Northern Illinois University, DeKalb, USA. He is currently a professor in the Department of Electronic Engineering, Dalian University of Technology. His research interests include non-Gaussian and non-stationary signal processing, radio frequency signal processing, and biomedical signal processing.

About the Author—FREDERIC MORAIN-NICOLIER received a master's degree in applied physics from Universite de Bourgogne in 1995 and Ph.D. degree in image processing at the same university in 2000. He is now an assistant professor at CRESTIC, Universite de Reims Champagne Ardenne (URCA). His research interest includes wavelets transform, images comparisons in biomedical and patrimonial imaging.

About the Author—SU RUAN received the Ph.D. degree in "Image Processing" from the University of Rennes 1, France, in 1993. She was Assistant Professor at the University of Caen from 1993 to 2003. Since 2003, she has been with the CReSTIC Laboratory at the University of Reims, where she is currently a full Professor. Her research interests include image segmentation, data fusion and pattern recognition, medical image processing.